PCCP

PAPER

View Article Online
View Journal

Cite this: DOI: 10.1039/c8cp02076k

Water transport and desalination through double-layer graphyne membranes†

Mojdeh Akhavan, [a] Jeremy Schofield [b] and Seifollah Jalili *[abc]

Non-equilibrium molecular dynamics simulations of water-salt solutions driven through single and double-layer graphyne membranes by a pressure difference created by rigid pistons are carried out to determine the relative performance of the membranes as filters in a reverse osmosis desalination process. It is found that the flow rate of water through a graphyne-4 membrane is twice that of a graphyne-3 membrane for both single and double-layer membranes. Although the addition of a second layer to a single-layer membrane reduces the membrane permeability, the double-layer graphyne membranes are still two or three orders of magnitude more permeable than commercial reverse osmosis membranes. The minimum reduction in flow rate for double-layer membranes occurs at a layer spacing of 0.35 nm with an AA stacking configuration, while at a spacing of 0.6 nm the flow rate is close to zero due to a high free energy barrier for permeation. This is caused by the difference in the environments on either side of the membrane sheets and the formation of a compact two-dimensional layer of water molecules in the interlayer space which slows down water permeation. The distribution of residence times of water molecules in the interlayer region suggests that at the critical layer spacing of 0.6 nm, a cross-over occurs in the mechanism of water flow from the collective movement of hydrogen-bonded water sheets to the permeation of individual water molecules. All membranes are demonstrated to have a high salt rejection fraction and the double-layered graphyne-4 membranes can further increase the salt rejection by trapping ions that have passed through the first membrane from the feed solution in the interlayer space.

Received 1st April 2018,
Accepted 27th April 2018

DOI: 10.1039/c8cp02076k

rsc.li/pccp

1. Introduction

With increasing global population growth and changes in climate caused by industrialization, the development of low-cost and energy-efficient methods for obtaining fresh water from the saline water of seas and oceans is among the most attractive scenarios for combating against water scarcity.[1] Currently, membrane-based technologies such as reverse osmosis (RO) nanofiltration, which uses the pressure difference across a membrane as a driving force to filter impurities, are widely used throughout the world for water treatment and desalination and much scientific activity has been devoted to improve the efficiency of RO processes by designing novel membrane materials.[2] Such membranes should allow water molecules to rapidly pass through them while at the same time efficiently blocking the passage of salts and other solutes. In this respect, nanomaterial-based membranes with their superior mechanical properties have many advantages over commercial membranes made from synthetic polymers such as polyamide thin film composite (TFC). Water molecules can flow at a high rate through the nanoporous structure of these materials, leaving behind solutes that permeate slowly due to the presence of high energy barriers to pass through the filtering membranes.[3]

Various types of nanomaterials have been examined as possible candidates for desalination membranes. Experiments[4,5] and molecular dynamics (MD) simulation studies[6–9] show that water can pass through carbon nanotubes (CNTs) at flow rates much higher than those obtained using current commercial membranes. The flow rate and the radial distribution of water molecules inside CNTs observed in MD simulations cannot be explained using Hagen–Poiseuille and Navier–Stokes classical equations and it is argued that the high flux of water molecules is due to the smooth and frictionless internal surface of narrow CNTs and the weak CNT–water interactions.[8,9] Another study explains the high flux to be a result of the velocity jump in a depletion region at the CNT–water interface, where water orientations with free OH bonds pointing to the nanotube wall weakens the hydrogen bonds.[7] This high flux rate has also been observed in MD simulations of arrays

[a] School of Nano-Science, Institute for Research in Fundamental Sciences (IPM), P.O. Box 19395-5531, Tehran, Iran
[b] Chemical Physics Theory Group, Department of Chemistry, University of Toronto, 80 Saint George Street, Toronto, Ontario, M5S 3H6, Canada
[c] Department of Chemistry, K. N. Toosi University of Technology, P. O. Box 15875-4416, Tehran, Iran. E-mail: sjalili@kntu.ac.ir; Tel: +98 21 22853649

† Electronic supplementary information (ESI) available. See DOI: 10.1039/c8cp02076k

of CNTs.[6] However, there are challenges associated with the usage of carbon nanotubes for desalination on an industrial scale. One problem is the difficulty of obtaining well-dispersed and properly aligned CNTs for membrane fabrication.[3] In addition, it is hard to prepare uniform samples of CNTs with diameters small enough (*i.e.* less that ~1 nm) to prevent ion permeation,[6] which causes the resulting membranes to have a low salt rejection at salt concentrations close to the salinity of seawater. MD simulations have shown that the addition of polar and charged functional groups at the entrance of larger diameter CNTs may help to improve rejection of salt at the cost of a reduction in the water flow rate due to strong electrostatic interactions between the charged functional groups and water molecules.[10]

Since water flux through CNT membranes increases with decreasing nanotube length (or membrane thickness),[9] ultrathin graphene sheets with nanopores have been suggested as convenient alternatives for CNTs.[11] Nanoporous graphene (NPG) has a high mechanical strength at large applied pressures[12] and water permeates NPG at a high rate.[11,13,14] In addition, by tuning the pore size and introducing functional groups, it can effectively reject ions in a selective manner.[11,15,16] However, for the realization of NPG membranes, a significant improvement in the techniques of pore carving in graphene sheet is required in order to produce high-density pores with a uniform size distribution.[17]

Graphyne compounds form another class of carbon allotropes with sp^2 and sp atoms which form nanosheets with the thickness of one atomic layer, similar to those in graphene.[18] In the structure of the γ-graphyne (or graphyne-*n*) phase, neighboring benzene rings are connected by *n* acetylenic linkages (see Fig. S1 in ESI†) and form triangular pores. For $n = 0$, the structure corresponds to graphene.[19] The first two members of graphyne-*n* compounds, *i.e.* graphyne ($n = 1$; the most stable member) and graphdiyne ($n = 2$) have interesting properties and various potential applications.[20] For instance, graphdiyne has been found to be a promising compound for nanoelectronics and hydrogen purification, as shown by first-principles electronic structure[21] and MD[22] studies. The next two members, graphyne-3 (or graphtriyne) and graphyne-4 have effective pore diameters of 3.8 and 5.4 Å,[23] suitable for desalination applications. MD simulations show that these structures have high permeability for water and can effectively block salts or other pollutants.[23–27] Moreover, the mechanical stability of the graphyne family and their high strength and stiffness makes them attractive candidates in RO nanofiltration.[23,26,28,29]

In this article, the performance of bilayer graphyne membranes in RO desalination is studied using non-equilibrium molecular dynamics simulations. A number of graphyne substructures have been successfully synthesized in laboratories[30–32] and the recent preparation of large areas of graphdiyne sheets with 3.61 cm^2 on copper substrate[33] has raised hopes for achieving the higher members of graphyne family in the near future. However, similar to the case of graphene sheets, it is probably hard to prepare these compounds as single layer sheets and the X-ray photoelectron spectra[33] show that the graphdiyne sheets are typically multilayer, defect-free films. Therefore, examining the effect of adding extra graphyne layers on water permeation and salt rejection through graphyne membranes may provide a useful guide for the optimization of graphyne membranes for desalination. Multilayer porous graphene sheets have been studied before[34,35] but to the best of our knowledge, this is the first work to study the effect of additional graphyne layers and other factors such as pore size, external pressure and layer-stacking for these fascinating structures. Our studies suggest that double-layer graphyne membranes are potentially useful for water desalination and that membranes with minimum loss in water flow rate due to additional graphyne layer(s) can be obtained by tuning parameters such as layer spacing and stacking.

2. Methods

A typical system setup for the non-equilibrium molecular dynamics (NEMD) simulations is shown in Fig. 1. The membrane is composed of 4 nm × 4 nm graphyne-3 (G3) or graphyne-4 (G4) sheets containing a single layer or two layers with AA (pore-aligned)

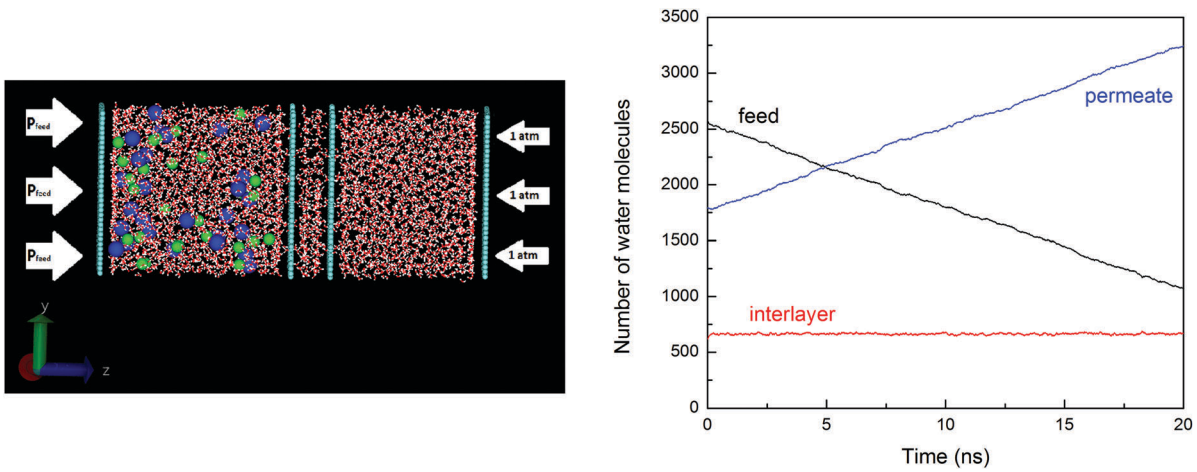

Fig. 1 The system setup with ions shown as van der Waals spheres (left) and the time evolution of the number of water molecules in different regions (right).

or AB stacking (Fig. S1, ESI†). The bond lengths in graphyne sheets were taken from ref. 19. The distance between two graphyne sheets was changed in the range of 0.35 to 2 nm, similar to those used in ref. 34 for graphene double layers. The membrane separates two reservoirs, one at the high-pressure (or feed) side containing saline water solution and the other at the low-pressure (or permeate) side containing pure water. The feed side initially contains 2600 water molecules, 28 Na^+ and 28 Cl^- ions to produce a salt concentration of 35 g L^{-1}, similar to the salinity of seawater. The space between two graphyne layers was initially hydrated with roughly 2500 water molecules in the interlayer and permeate regions in total, with varying numbers for different systems.

The pressure difference across the membrane was produced by using two rigid movable graphene walls (or pistons) on either side of the reservoirs (normal to the flow direction) and applying external forces to the walls to produce a pressure of 0.1 MPa (1 atm) at the permeate side and P at the feed side. The external forces (F) were applied along the $+z$ direction on each carbon atom of the feed piston and along the $-z$ direction on each carbon atom of the permeate piston (see Fig. 1). Pressure values in the range of 50–200 MPa were used, which are much higher than the typical values in real commercial NF systems (which are typically on the order of a few MPa), but since the flux of water molecules through the membrane depends linearly on the external pressure, the permeability values obtained scale appropriately at low pressures. The initial distance separating the external pistons was set to 10 nm and the feed membrane was initially positioned at the midpoint between the two pistons. Cartesian coordinates were defined with the membrane and piston sheets in the xy plane and the flow direction along the z axis. Periodic boundary conditions (PBC) were applied in the x and y dimensions. The dimensions of graphene pistons were 4.2 nm × 4.2 nm, equal to the simulation box edge lengths in x and y directions.

All simulations and subsequent analyses were performed using the Gromacs simulation package version 4.6.1.[36] The equations of motion were integrated using the leapfrog algorithm with a simulation time step of 1.0 fs. Carbon atoms in graphyne were treated as neutral Lennard-Jones particles with interaction parameters ε = 0.3612 kJ mol^{-1} and σ = 0.34 nm.[24] The same parameters were used for piston atoms interacting with water molecules and ions. The SPC/E model[37] was used for water molecules and the OPLS parameters taken from ref. 23 were applied for Na^+ and Cl^- ions. Lorentz–Berthelot combining rules[38] were used to obtain Lennard-Jones parameters for unlike particles, with a short-range cutoff of 1.4 nm. Electrostatic interactions were treated using the PME method[39] with a real space cutoff of 1.4 nm and a reciprocal grid spacing of 0.12 nm. To apply PME on the xy-periodic system, the PBC size in z direction was set to be three times the z dimension of the box and the 3D-PBC potential and force corrections were used.[40] During the simulations, membrane atoms were kept frozen at their initial positions. This has been shown to have a negligible impact on the desired properties such as water flow.[11,41] The internal geometry of water molecules was constrained by using the SETTLE algorithm.[42]

In all simulations, the total energy of the system was first minimized and then the system was equilibrated for 200 ps with an external pressure of 0.1 MPa on both pressure pistons to reach the equilibrium water density ($\sim$1 g mL^{-1}). During the equilibration phase, a temperature of 300 K was maintained using the velocity rescaling method[43] with a time constant of 0.1 ps. To remove excess energy from the system, the fluid particles (water and ions) and piston atoms were separately thermostatted. Our test simulations with water molecules' temperature uncontrolled, as suggested in ref. 35, did not show any change in the calculated water flow rate, so the applied thermostat does not disturb the dynamics of water molecules. The production simulations were then performed for 40 ns at P = 50 MPa and for 20 ns at other external pressures and the coordinates were saved every 1 ps. For some representative cases, the simulations were performed for three independent sets of initial conditions to verify that the starting positions of ions have no effect on the results. The trajectories were analyzed to obtain the properties discussed in the Results section.

3. Results and discussion

Under non-equilibrium conditions with a hydrostatic pressure difference between the pistons, water molecules move in $+z$-direction from the feed solution to the permeate side. As Fig. 1 (right) shows, the system rapidly reaches a steady-state in which the number of water molecules in the feed side decreases at a constant rate and the number of water molecules in the permeate side increases at the same rate, while the interlayer region maintains an almost constant number of water molecules. This trend indicates the negligible effect of the increasing salt concentration in the feed solution on water flow rate, as observed in the desalination simulations using NPG membranes.[11,34]

Fig. S2(a) (ESI†) shows a typical plot of the number of water molecules in the permeate reservoir as a function of the simulation time. This number increases with time and attains a plateau value at long times due to the lack of water molecules in feed solution in our dead-end RO simulation system. The slope of this plot in the linear regime gives the number flow rate (F) for water molecules. In order to obtain F, a reference or final time (t_f) is required to calculate the slope from t = 0 to t_f. Using the same arguments as in ref. 34 for NPG membranes, we take t_f as $t_{1/5}$ (the time when 20% of water molecules initially in feed solution have passed through the membrane) for graphyne-3 and $t_{1/2}$ (when 50% of feed water molecules have permeated) for graphyne-4. Dividing F by the membrane area (A) gives the water flux (J) per unit area across the membrane. The flux depends linearly on the applied pressure, as shown in Fig. S2(b) (ESI†). A linear regression fitting gives the water permeability of the membrane as the slope of a plot of the flux *versus* the difference in applied pressure. The permeabilities of single-layer G3 and G4 membranes are found to be 0.0025 and 0.0060 m MPa^{-1} s^{-1} respectively, which are in agreement with previous MD studies.[23,27] For double-layer membranes, the permeability is reduced by up to 50% depending on the

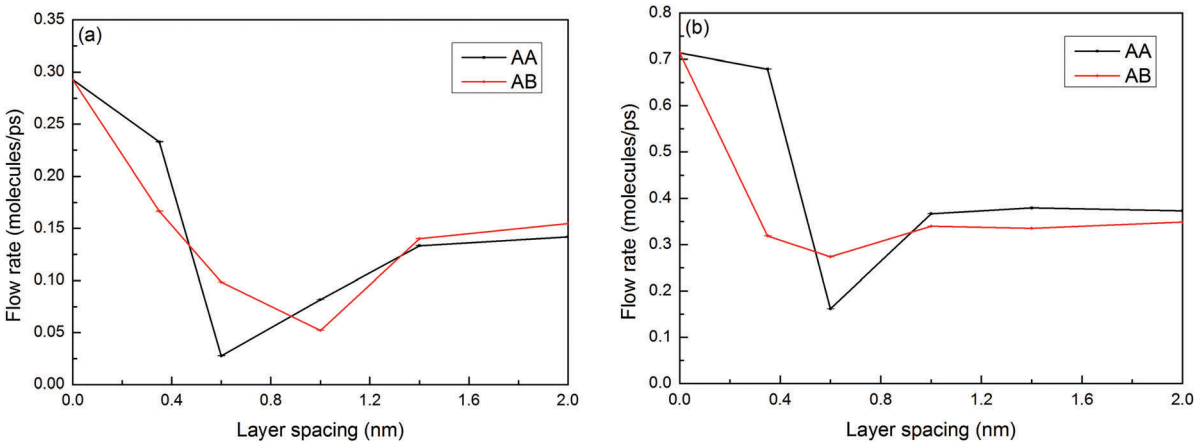

Fig. 2 Water flow rates through AA and AB-stacked layers of graphyne-3 (a) and graphyne-4 (b) as a function of layer spacing at an applied pressure of 200 MPa.

layer spacing. Since the permeability is defined as a material property of the homogenous membrane,[35] we cannot directly compare the permeability of a membrane composed of two distinct layers with that of a single layer membrane. However, even considering the possible reduction due to the additional layer, the graphyne membranes are still two to three orders of magnitude more permeable than the commercial RO membranes.

We now consider the effect of the layer spacing and the structural alignment of pores on the flow rate of water through bilayer graphyne membranes. Fig. 2 shows the changes in the number flow rate F as a function of layer separation (D) for AA and AB-stacked graphyne layers at 200 MPa. We note that qualitatively similar data have been obtained at other pressures. The values on the vertical axes (zero D) are for single layer membranes. The flow rate decreases with increasing layer separation up to separations of D = 0.6 nm after which the flow rate begins to increase. For layer spacings larger than $\sim$1 nm, the flow rate reaches a constant value of about half of the flow rate for the corresponding single-layer membrane. The flow rates for graphyne-4 are about twice the values for graphyne-3 for all layer separations. Regarding the effect of pore alignment, Fig. 2 shows that the difference between the flow rates for AA and AB stacking is larger at smaller D values. In particular, in the AA-stacked graphyne-3 bilayer with D = 0.6 nm, the flow rate drops near zero. For D = 0.35 nm, however, it only falls by less than 20% compared to AB stacking. For graphyne-4, AA and AB flow rates show a greater difference at D = 0.35 nm. The results are in qualitative agreement with those for bilayer graphene membranes, for which the flow rate increases with the applied pressure and it does not depend on layer separation and pore offset at large spacings.[34]

To further understand the effect of layer spacing the mass density profile $\rho(z)$ and free energy profile $G(z) = -k_BT\ln[\rho(z)]$ of water molecules along the flow direction have been computed. As Fig. S3 (ESI†) shows, far from the membrane the density corresponds to its bulk value, while strong layering of water molecules is evident near the membrane surfaces. Note that the peaks in the density profile on the feed side are usually higher due to the greater hydrostatic pressure on that side. There are also small concentration peaks right before and after the graphyne-3 surfaces indicating binding sites across the membrane stabilizing the passage of water molecules as a single-file chain.[13,24,25] For graphyne-4 with larger pores, these peaks turn into shoulders. This is the only major difference between G3 and G4 membranes and so we have omitted the density profiles for G4 bilayers for brevity. At the smallest layer separation D, the interlayer region can only accommodate a few water molecules (20 and 10 molecules on average for the AA and AB stacking geometries, respectively), which is reflected by the small peak in the density in the range of 15 to 15.35 nm. When D is increased to 0.6 nm, there is enough room for a strong single pseudo two-dimensional layer of water molecules to be formed which may prevent molecules from easily passing through the membrane. For larger D's, the density profile in the interlayer region resembles the bulk solution density on the feed side.

The effective (free) energy barriers for water permeation can be estimated using the free energy profiles in Fig. 3. For the graphyne-3 single-layer membrane, the energy barrier is about $2.9k_BT$, which is close to the values reported by others.[24,25] The barrier is mainly caused by the energetic penalty associated with hydrogen bond breakage as water molecules pass through the membrane pores. As the hydrogen bonding profile in Fig. S4 (ESI†) shows, each water molecule at the feed side has $\sim$3.5 hydrogen bonds, which is in agreement with the value of 3.59 obtained in equilibrium MD simulations of SPC/E water model[44] but some of these hydrogen bonds should be broken before water could pass through the membrane. For the single-layer G4 membrane system, the energy barrier is $\sim 1.3k_BT$ lower and this difference in barriers is consistently observed for all bilayer membranes. The decreased barrier for G4 can be justified by the smaller drop in the number of hydrogen bonds upon passing the larger pores (see Fig. S4, ESI†). Similar to the case for density profiles, we have only included the free energy profiles for G3 bilayer membranes.

As seen in Fig. 2, there are two different regimes for the interlayer distance (D) dependence of the flow rate: $D > 0.6$ nm

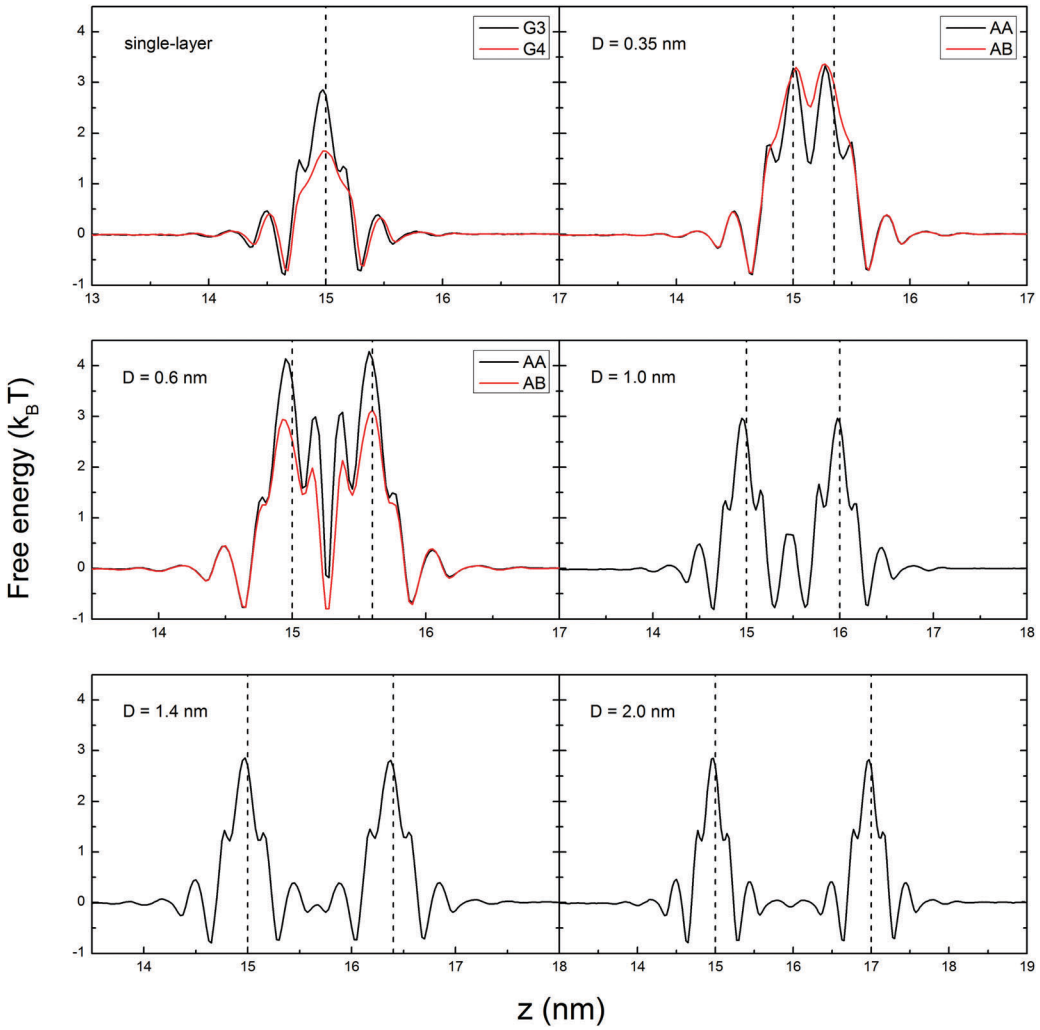

Fig. 3 Steady state free energy profiles for water molecules permeating through single layer and double-layer graphyne membranes. The double-layer plots are for graphyne-3 and the dashed lines indicate the positions of membrane sheets.

and $D \leq 0.6$ nm. This non-linear behavior can be explained based on the free energy profiles shown in Fig. 3. After a water molecule overcomes the energy barrier for passing through the pores of the first membrane, it faces an additional energy barrier for moving in the interlayer space.[45] In other words, in order to permeate the molecule has to overcome an "entrance" and an "exit" barrier, each at one of the graphyne sheets. For the last three systems ($D > 0.6$ nm), the water structure on either side of the first graphyne sheet is similar because the large interspace volume allows the water molecules to assume a bulk-like structure. So the entrance barrier is similar to the single layer case (Fig. 3). A similar situation holds for the second graphyne sheet, so there is an additional "exit barrier" equal to the entrance barrier and the flow rate for these systems are about half the value for the single-layer membrane, which is consistent with the resistance-in-series model observed in bilayer NPG membranes.[34]

For the two smallest layer spacing values (0.35 and 0.6 nm), the situation is quite different. These systems have higher entrance barriers compared to the single-layer system because the water faces a different environment when it enters the interlayer region (Fig. 4). The difference in water structure has been recognized as a source of higher energy barrier for water passage through carbon nanotubes compared to a porous graphene sheet.[13] For $D = 0.35$ nm however, since the interlayer region can accommodate only a few water molecules (Fig. 4), once a new water molecule passes through the first membrane it can easily reach the second one and permeate. In other words, this system has a lowest exit barrier among the double-layer systems, so it shows the minimum reduction in flow rate with respect to the system with a single membrane layer.

The most special case occurs for the spacing of 0.6 nm, which shows a very small flow rate. This system has a much larger entrance barrier due to the difference in water structures across the membrane (Fig. 4) and a nearly complete water depletion in the region next to the membrane surface (with a density near zero, Fig. S3, ESI†). In addition, it is very hard for a water molecule to pass through the compact pseudo-two-dimensional layer of water molecules which is formed in the interlayer space. As Fig. 4 (lower row) shows, the water molecules

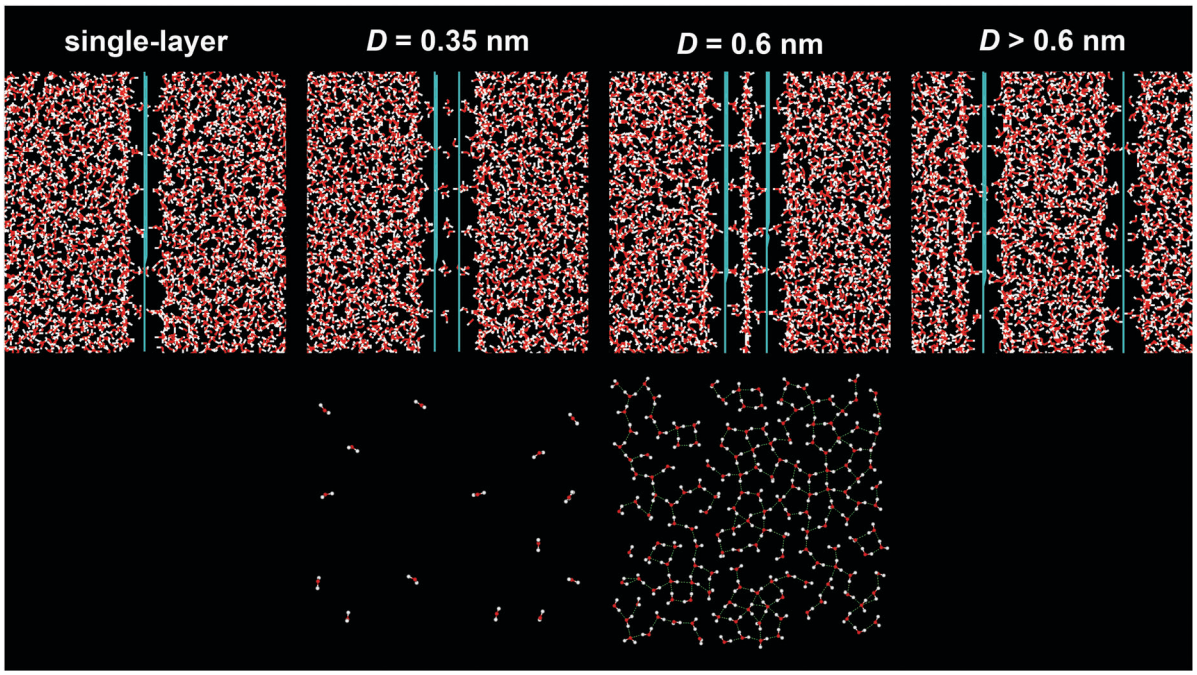

Fig. 4 Structure of water molecules on either side of the graphyne membranes for different spacing (D) values. The lower row shows the structure of water molecules in the interlayer region in the plane normal to the direction of water flow.

form a network of hydrogen bonds in the plane normal to the direction of water flow, so that an incoming water molecule has to overcome a large energy barrier to pass through this layer and enter the permeate side. Having high entrance and exit barriers, the water molecules show the lowest flow rate for this layer spacing value.

The properties of water molecules which permeate a bilayer membrane have been further studied by estimating the average residence time (t_{res}) of water molecules, which is calculated as the difference in times when a given molecule enters and then subsequently exits the interlayer region. The averaging is performed for all water molecules which are initially in the feed solution and permeate at some time during the simulation. Fig. 5a shows the results for different layer spacing values. The residence times for bilayers membranes of graphyne-3 are more sensitive to changes in the interlayer separation D than those for graphyne-4. As expected, the residence time increases as the interlayer distance increases. One exception is for bilayers separated by 0.6 nm, in which the lowest average residence time is observed in spite of having the slowest water flow. The lack of correlation between residence times and flow rates has been also reported for double layer NPG membranes and it has been argued that the flow rate is controlled by the energy barrier, rather than residence time.[34] On the same basis,

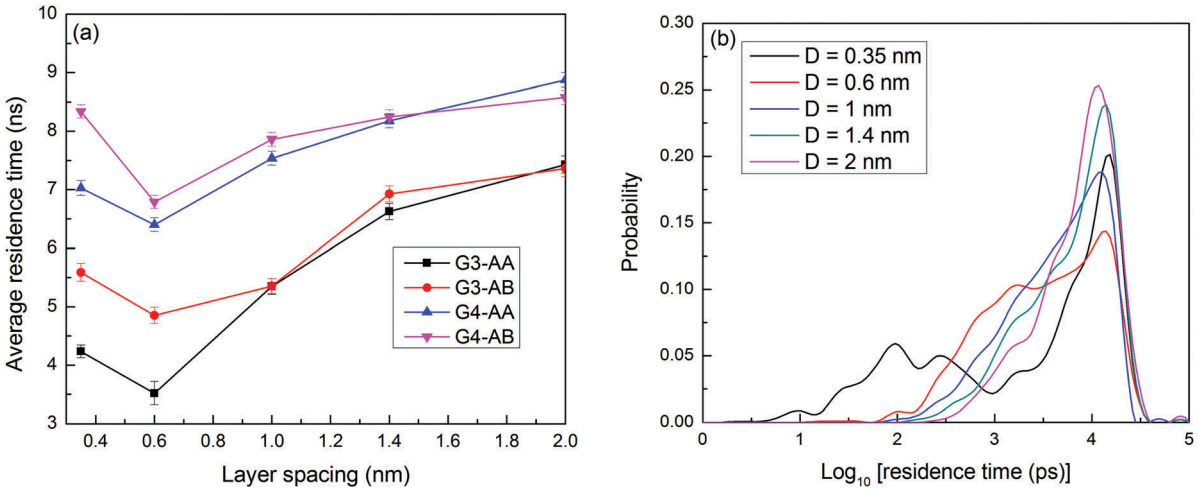

Fig. 5 (a) Average residence times in the interlayer region as a function of layer spacing for water molecules passing through bilayer graphyne membranes with different geometries. (b) The probability distribution of residence times for different values of layer spacing (graphyne-3, AB stacking).

the changes in t_{res} with D for AA and AB stacking do not show any correlation with the changes in flow rates; AA stacking has always a lower t_{res} than AB.

Distribution of residence times (Fig. 5b) can be used to understand the mechanism of water flow in the interlayer region. For all values of the layer separation, there is a peak in the distribution of residence times corresponding to a relatively long residence time on the order of 10 ns. At two smallest D's however, there is a broader distribution of t_{res} values, indicating that an important fraction of water molecules pass through the interlayer region with a rate of up to two orders of magnitude greater than that of other water molecules. This reflects a difference in the mechanism of water flow for these systems. When the distribution shows only one peak, which is nearly the case for $D > 0.6$ nm, we can suppose that water molecules which enter the interlayer region at a same time will leave it together and so they can move as a single hydrogen-bonded sheet of water molecules.[35] But when the distribution is broad, the water molecules cannot move at a same speed. Every single molecule has to pave its own way through the interlayer space to reach the second membrane, so the structure of water molecules in the interlayer region plays a significant role and directly affects the flow rate: for $D = 0.6$ nm with a compact, hydrogen-bonded plane of water molecules in the interlayer space, it is a difficult way and the flow rate is very low accordingly. The change in the distribution of residence times at a critical layer spacing which can be a sign of a cross-over in the mechanism of permeation dynamics has also been reported for the double-layer graphene membranes.[34]

Turning now to the performance of single and double-layer graphyne membranes for the desalination of seawater, a common measure of performance is the salt rejection fraction (usually expressed in %), defined as $R = 1 - N(t_f)/N_0$, where $N(t_f)$ is the average number of Na^+ and Cl^- ions in the permeate solution at t_f and N_0 is the number of ions in feed solution at the beginning of simulation. With graphyne-3 membranes, R is always 1 (or 100%) at all pressures and layer spacing values. For graphyne-4 membranes with larger pores however, as expected, R is lower. Both layer spacing and applied pressure can impact the value of R for G4 membranes. The effect of the increased layer spacing, which is only visible at high applied pressures, as we will see shortly, is to improve the salt rejection percent (Fig. S5a, ESI†). The higher applied pressures on the other hand lead to a lower value of R for a single-layer graphyne-4 membrane: it is 98% at the applied pressure of 50 MPa and reaches a value of 96% at 200 MPa (Fig. S5b, ESI†). The range of salt rejection values and the decrease in R at higher pressures agree with other desalination simulations using graphyne membranes.[23,25,27]

The difference characteristics of single and double layer membranes can be better observed in the ionic density profiles shown in Fig. 6. For the single-layer graphyne-3 membrane (Fig. 6a), the profile of the density of sodium ions has a peak at a distance of 0.5 nm from the membrane surface in the feed solution, corresponding to an interfacial region comprised of ions separated from the surface by a layer of water molecules. The profile of the chloride ions has two peaks 0.4 nm and 0.6 nm away from the membrane surface for direct and water-separated graphyne-ion contacts, respectively.[46] Note that the density of ions in the permeate region ($z > 15$) is zero, indicating that the graphyne-3 membrane is completely impermeable to salt ions. In contrast to graphyne-3, for single-layer graphyne-4 membrane, the ions have non-zero density in the permeate solution, as shown in Fig. 6b, but when two graphyne-4 membranes are used, the ion concentration gradually decreases from the feed to the interlayer region and reaches to near zero in the permeate ($z > 16$) solution (Fig. 6c). So the doubling in the number of filters leads to a lower salt rejection for the double-layer membranes.

In terms of the two well-known requirements for an efficient desalination membrane, *i.e.* having high permeability and high salt rejection, we can compare different membrane systems of nanomaterials and conventional types.[11,27] As shown in Fig. 7, nanoporous graphene (NPG) with hydrogenated (graphene-H) and hydroxylated (graphene-OH) pore edges are among the effective membranes with high permeability and salt rejection. As shown in previous MD simulations and confirmed in our work,[25–27] graphyne-4 membranes have a higher permeability than NPG membranes but at the cost of lower salt rejection. However, if we add an additional layer to these membranes at a carefully chosen distance, we will reach a high salt rejection (at applied pressures lower than 50 MPa which are common in practical applications), without losing the high permeability. We should also note that there are other factors which are

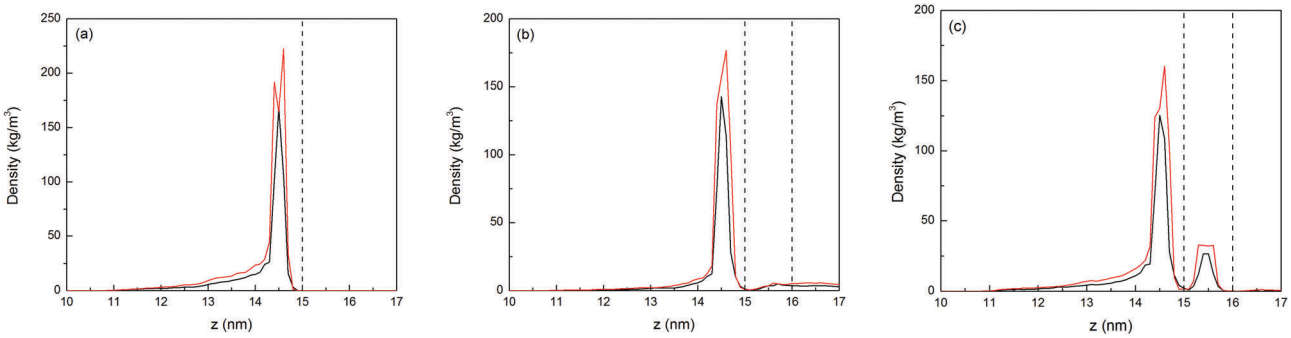

Fig. 6 Density profiles for Na^+ (black lines) and Cl^- (red lines) along the z-axis for single-layer graphyne-3 (a), single-layer graphyne-4 (b) and double-layer (AA, D = 1 nm) graphyne-4 membrane (c). Dashed lines indicate the positions of membrane sheets.

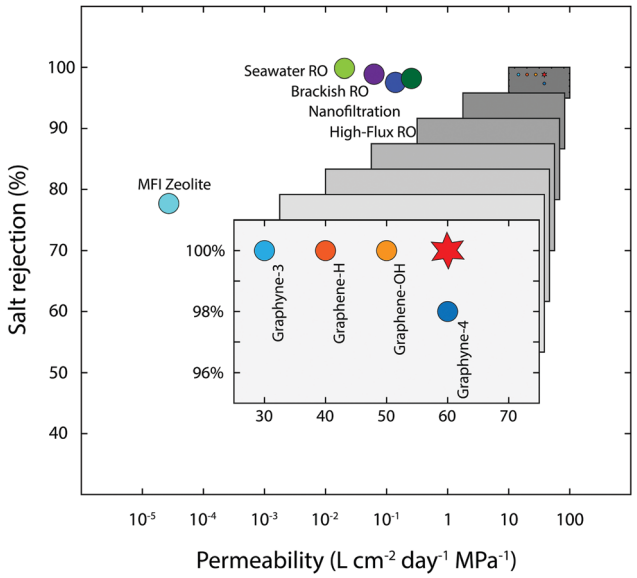

Fig. 7 A comparison between different desalination membranes. This is an updated version of the plot used in ref. 11 and 27. The red star denotes our double-layered graphyne-4 membranes.

important in determining the suitability of nanomaterial-based membranes for using in desalination systems, such as the dependence of permeability on salt concentration and the size and weight of the membrane.[47] Our double-layered graphyne membranes show similar properties to those of double-layer graphene membranes,[34] such as the best case being with small layer separation and aligned pores and reduction in salt rejection with increasing the applied pressure, but the pressure-dependence of salt rejection is weaker and the permeability is higher in our systems. As for the size and weight, based on the same arguments which are given for NPG membranes,[34] we can fabricate graphyne membranes much thinner than conventional polyamide films and still reach a same permeability and salt rejection.

4. Conclusions

The results obtained from our non-equilibrium molecular dynamics simulations can provide some useful guidelines for the future fabrication of graphyne membranes for seawater desalination. Firstly, the membranes composed of graphyne-4 have higher water flow rates than graphyne-3 membranes while being equally effective in salt rejection. Next, as for the layer spacing and configuration in double-layer membranes, flow rate data shows that the best case is obtained with a layer spacing of $\sim$0.35 nm (similar to graphite), especially with the AA stacking configuration. The flow rate for this spacing is very close to the single-layer value and it will have a high salt rejection at low applied pressures. However, if the synthesized double layers at this distance are not stable, then care must be taken to avoid the layer spacing of 0.6 nm where the flow rate is dramatically reduced due to confinement effects. In this case, a spacing of 1 nm or higher (which can be achieved by using spacers or intercalants) would be a reasonable choice to gain a moderate water flow rate and high salt rejection. Finally, in this work we have focused on double-layers to explore the effect of additional layers on the performance of graphyne membranes. Extension to more than two layers can be the considered as the next step in predicting the properties of multi-layer graphyne membranes.

Conflicts of interest

There are no conflicts of interest to declare.

Acknowledgements

This work has been supported (project number 93005246) by Iran National Science Foundation (INSF). Calculations were performed using WestGrid (www.westgrid.ca) and Compute Canada Calcul Canada (www.computecanada.ca) computing facilities.

References

1 J. R. Werber, A. Deshmukh and M. Elimelech, The critical need for increased selectivity, not increased water permeability, for desalination membranes, *Environ. Sci. Technol. Lett.*, 2016, **3**, 112–120.
2 J. R. Werber, C. O. Osuji and M. Elimelech, Materials for next-generation desalination and water purification membranes, *Nat. Rev. Mater.*, 2016, **1**, 16018, DOI: 10.1038/natrevmats.2016.18.
3 S. Daer, J. Kharraz, A. Giwa and S. W. Hasan, Recent applications of nanomaterials in water desalination: A critical review and future opportunities, *Desalination*, 2015, **367**, 37–48.
4 J. K. Holt, H. G. Park, Y. Wang, M. Stadermann, A. B. Artyukhin, C. P. Grigoropoulos, A. Noy and O. Bakajin, Fast mass transport through sub-2-nanometer carbon nanotubes, *Science*, 2006, **312**, 1034–1037.
5 K. Gethard, O. Sae-Khow and S. Mitra, Water desalination using carbon-nanotube-enhanced membrane distillation, *ACS Appl. Mater. Interfaces*, 2011, **3**, 110–114.
6 B. Corry, Designing carbon nanotube membranes for efficient water desalination, *J. Phys. Chem. B*, 2008, **112**, 1427–1434.
7 S. Joseph and N. R. Aluru, Why are carbon nanotubes fast transporters of water?, *Nano Lett.*, 2008, **8**, 452–458.
8 M. Majumder and B. Corry, Anomalous decline of water transport in covalently modified carbon nanotube membranes, *Chem. Commun.*, 2011, **47**, 7683–7685.
9 L. Wang, R. S. Dumont and J. M. Dickson, Nonequilibrium molecular dynamics simulation of water transport through carbon nanotube membranes at low pressure, *J. Chem. Phys.*, 2012, **137**, 044102.
10 B. Corry, Water and ion transport through functionalised carbon nanotubes: Implications for desalination technology, *Energy Environ. Sci.*, 2011, **4**, 751–759.
11 D. Cohen-Tanugi and J. C. Grossman, Water desalination across nanoporous graphene, *Nano Lett.*, 2012, **12**, 3602–3608.
12 D. Cohen-Tanugi and J. C. Grossman, Mechanical strength of nanoporous graphene as a desalination membrane, *Nano Lett.*, 2014, **14**, 6171–6178.

13 M. E. Suk and N. R. Aluru, Water transport through ultrathin graphene, *J. Phys. Chem. Lett.*, 2010, **1**, 1590–1594.
14 C. Zhu, H. Li and S. Meng, Transport behavior of water molecules through two-dimensional nanopores, *J. Chem. Phys.*, 2014, **141**, 18C528.
15 K. Sint, B. Wang and P. Král, Selective ion passage through functionalized graphene nanopores, *J. Am. Chem. Soc.*, 2008, **130**, 16448–16449.
16 D. Konatham, J. Yu, T. A. Ho and A. Striolo, Simulation insights for graphene-based water desalination, *Langmuir*, 2013, **29**, 11884–11897.
17 D. Cohen-Tanugi and J. C. Grossman, Nanoporous graphene as a reverse osmosis membrane: recent insights from theory and simulation, *Desalination*, 2015, **366**, 59–70.
18 R. H. Baughman, H. Eckhardt and M. Kertesz, Structure–property predictions for new planar forms of carbon: Layered phases containing sp^2 and sp atoms, *J. Chem. Phys.*, 1987, **87**, 6687–6699.
19 N. Narita, S. Nagai, S. Suzuki and K. Nakao, Optimized geometries and electronic structures of graphyne and its family, *Phys. Rev. B: Condens. Matter Mater. Phys.*, 1998, **58**, 11009–11014.
20 Q. Peng, A. K. Dearden, J. Crean, L. Han, S. Liu, X. Wen and S. De, New materials graphyne, graphdiyne, graphone, and graphane: Review of properties, synthesis, and application in nanotechnology, *Nanotechnol., Sci. Appl.*, 2014, **7**, 1–29.
21 Y. Jiao, A. Du, M. Hankel, Z. Zhu, V. Rudolph and S. C. Smith, Graphdiyne: a versatile nanomaterial for electronics and hydrogen purification, *Chem. Commun.*, 2011, **47**, 11843–11845.
22 S. W. Cranford and M. J. Buehler, Selective hydrogen purification through graphdiyne under ambient temperature and pressure, *Nanoscale*, 2012, **4**, 4587–4593.
23 S. Lin and M. J. Buehler, Mechanics and molecular filtration performance of graphyne nanoweb membranes for selective water purification, *Nanoscale*, 2013, **5**, 11801–11807.
24 J. Kou, X. Zhou, Y. Chen, H. Lu and F. Wu, Water permeation through single-layer graphyne membrane, *J. Chem. Phys.*, 2013, **139**, 064705.
25 M. Xue, H. Qiu and W. Guo, Exceptionally fast water desalination at complete salt rejection by pristine graphyne monolayers, *Nanotechnology*, 2013, **24**, 505720.
26 C. Zhu, H. Li, X. C. Zeng, E. G. Wang and S. Meng, Quantized water transport: ideal desalination through graphyne-4 membrane, *Sci. Rep.*, 2013, **3**, 3163.
27 J. Kou, X. Zhou, H. Lu, F. Wu and J. Fan, Graphyne as the membrane for water desalination, *Nanoscale*, 2014, **6**, 1865–1870.
28 S. W. Cranford and M. J. Buehler, Mechanical properties of graphyne, *Carbon*, 2011, **49**, 4111–4121.
29 Y. Yang and X. Xu, Mechanical properties of graphyne and its family: a molecular dynamics investigation, *Comput. Mater. Sci.*, 2012, **61**, 83–88.
30 M. M. Haley, S. C. Brand and J. J. Pak, Carbon networks based on dehydrobenzoannulenes: synthesis of graphdiyne substructures, *Angew. Chem., Int. Ed. Engl.*, 1997, **36**, 836–838.
31 J. M. Kehoe, J. H. Kiley, J. J. English, C. A. Johnson, R. C. Petersen and M. M. Haley, Carbon networks bases on dehydrobenzoannulenes. 3. Synthesis of graphyne substructures, *Org. Lett.*, 2000, **2**, 969–972.
32 M. M. Haley, Synthesis and properties of annulenic subunits of graphyne and graphdiyne nanoarchitectures, *Pure Appl. Chem.*, 2008, **80**, 519–532.
33 G. Li, Y. Li, H. Liu, Y. Guo, Y. Li and D. Zhu, Architecture of graphdiyne nanoscale films, *Chem. Commun.*, 2010, **46**, 3256–3258.
34 D. Cohen-Tanugi, L.-C. Lin and J. C. Grossman, Multilayer nanoporous graphene membranes for water desalination, *Nano Lett.*, 2016, **16**, 1027–1033.
35 J. Muscatello, F. Jaeger, O. K. Matar and E. A. Müller, Optimizing water transport through graphene-based membranes: insights from nonequilibrium molecular dynamics, *ACS Appl. Mater. Interfaces*, 2016, **8**, 12330–12336.
36 B. Hess, C. Kutzner, D. van der Spoel and E. Lindahl, GROMACS 4: algorithms for highly efficient, load-balanced, and scalable molecular simulation, *J. Chem. Theory Comput.*, 2008, **4**, 435–447.
37 H. J. C. Berendsen, J. R. Grigera and T. P. Straatsma, The missing term in effective pair potentials, *J. Phys. Chem.*, 1987, **91**, 6269–6271.
38 M. P. Allen and D. J. Tildesley, *Computer simulation of liquids*, Oxford University Press, Oxford, 1989.
39 U. Essmann, L. Perera, M. L. Berkowitz, T. Darden, H. Lee and L. G. Pedersen, A smooth particle mesh Ewald method, *J. Chem. Phys.*, 1995, **103**, 8577–8593.
40 I. C. Yeh and M. L. Berkowitz, Ewald summation for systems with slab geometry, *J. Chem. Phys.*, 1999, **111**, 3155–3162.
41 M. E. Suk and N. R. Aluru, Effect of induced electric field on single-file reverse osmosis, *Phys. Chem. Chem. Phys.*, 2009, **11**, 8614–8619.
42 S. Miyamoto and P. A. Kollman, SETTLE: An analytical version of the SHAKE and RATTLE algorithm for rigid water models, *J. Comput. Chem.*, 1992, **13**, 952–962.
43 G. Bussi, D. Donadio and M. Parrinello, Canonical sampling through velocity rescaling, *J. Chem. Phys.*, 2007, **126**, 014101.
44 D. van der Speol, P. J. van Maaren, P. Larsson and N. Tîmneanu, Thermodynamics of hydrogen bonding in hydrophilic and hydrophobic media, *J. Phys. Chem. B*, 2006, **110**, 4393–4398.
45 M. E. Suk, A. V. Raghunathan and N. R. Aluru, Fast reverse osmosis using boron nitride and carbon nanotubes, *Appl. Phys. Lett.*, 2008, **92**, 133120.
46 A. I. Frolov, A. G. Rozhin and M. V. Fedorov, Ion interactions with the carbon nanotube surface in aqueous solution: understanding the molecular mechanism, *ChemPhysChem*, 2010, **11**, 2612–2616.
47 M. Thomas and B. Corry, A computational assessment of the permeability and salt rejection of carbon nanotube membranes and their application to water desalination, *Philos. Trans. R. Soc., A*, 2016, **374**, 20150020.